Available online at www.sciencedirect.com
ScienceDirect
International Journal of Rock Mechanics & Mining Sciences 45 (2008) 831–847
International Journal of Rock Mechanics and Mining Sciences
www.elsevier.com/locate/ijrmms

An exact implementation of the Hoek–Brown criterion for elasto-plastic finite element calculations

Johan Clausen, Lars Damkilde*

Esbjerg Institute of Technology, Aalborg University, Niels Bohrs Vej 8, 6700 Esbjerg, Denmark

Received 28 November 2006; received in revised form 11 October 2007; accepted 12 October 2007
Available online 26 November 2007

Abstract

A simple stress update algorithm for generalised Hoek–Brown plasticity is presented. It is intended for use in elasto-plastic finite element computations and utilises the return mapping concept for computing the stress increment belonging to a given increment in strain at a material point. In the algorithm all manipulations are carried out in principal stress space, where the Hoek–Brown failure criterion has a very simple form compared to its formulation in general stress space. In principal stress space it is also simple to determine whether the stress should be returned to one of the edges or to the apex of the yield surface and to form the constitutive matrices. As opposed to earlier finite element implementations of Hoek–Brown plasticity the exact criterion is used, i.e. no rounding of the yield surface corners or edges is attempted. Numerical examples and a comparison with an often used method for dealing with the corner singularities indicates the efficiency of the presented.

Keywords: Generalised Hoek–Brown criterion; Plastic stress update; Return mapping; Non-linear FEM

1. Introduction

Since it first appeared in [1] the Hoek–Brown failure criterion has been widely used for estimating the bearing capacity and deformation of rock masses. The criterion itself has evolved over time and its most recent form can be found in [2]. One of the reasons for the popularity of the failure criterion is due to the fact that the material parameters can be estimated based on simple field observations coupled with knowledge of the uniaxial compressive strength of the intact rock material, see e.g. [3–5]. The Hoek–Brown failure criterion is one of the few non-linear failure criteria that are used for practical civil engineering purposes and a number of analytical and semi-analytical solutions to practical problems have been developed. Some recent examples are found in Refs. [6–10]. Here the term "non-linear failure criterion" refers to the fact that the material strength depends on the hydrostatic pressure in a non-linear manner.

The most versatile method of performing elastic–plastic calculations on arbitrary geometries is the finite element method. In this context the Hoek–Brown failure criterion is treated as a yield criterion, i.e. the material experiences plastic flow when the stress state is located on the yield criterion. As the linear Mohr–Coulomb criterion is implemented in many commercial codes, this criterion is often used instead of the Hoek–Brown criterion. The challenge is then to determine appropriate Mohr–Coulomb parameters. These are usually found by fitting the Mohr–Coulomb criterion to the Hoek–Brown criterion within an appropriate stress range, sometimes in conjunction with a tension cut-off, i.e. a Rankine criterion. Examples of these fitting procedures can be found in [11–13,2].

Lower and upper bounds for the limit load for an associated Hoek–Brown material in plane strain are computed in Ref. [14], where the criterion is slightly modified in order to avoid the singularity present at the apex.

In the literature only a few examples of implementation of the Hoek–Brown criterion in an elasto-plastic finite

*Corresponding author. Tel.: +45 79 12 76 48; fax: +45 75 45 36 43.
E-mail address: ld@aaue.dk (L. Damkilde).

1365-1609/$ - see front matter © 2007 Elsevier Ltd. All rights reserved.
doi:10.1016/j.ijrmms.2007.10.004

element context are given. The ones that are known to the authors are found in Refs. [15,16]. Both references introduce a rounding of the corners in order to avoid numerical difficulties. This means that the results obtained with these methods in general do not converge toward the exact solutions. In both references a non-associated flow rule has been adopted in order to better capture the dilatative behaviour of the rock mass.

Some commercial finite element codes incorporate the Hoek–Brown criterion, but these implementations are also based on a rounding of the corners and the apex. Another method of dealing with the corner singularities is to approximate the criterion with the Drucker–Prager criterion for corner stress points, see e.g. [17,18].

This paper presents a plastic stress update algorithm for the exact generalised Hoek–Brown criterion including the apex and corner singularities. The algorithm is intended for use with the elasto-plastic finite element method and examples of this use will be given. The plastic flow rule is taken to be non-associated with a plastic potential which is similar to the yield criterion. Perfect plasticity and isotropic linear elasticity are assumed. The stress update algorithm belongs to the class of algorithms termed return mapping, backward euler or implicit integration.

Numerical examples that compare the results of other methods with results obtained from the presented method will be given. Also the added efficiency of the presented method compared to that of the Drucker–Prager corner approximation will be quantified.

The stress update algorithm code used in this paper is available from the authors in a MatLab or a Fortran version.

2. The Hoek–Brown failure criterion

The material parameters for the rock mass are derived from two parameters relating to the intact rock material, coupled with two other parameters which characterise the quality of the in situ rock mass. The intact rock parameters are the uniaxial compressive strength of the intact rock material, σ_{ci}, and the petrographic constant, m_i. Examples of the latter can be found in e.g. Refs. [4,19]. The first in situ parameter is the Geological Strength Index, GSI, which is a qualitative classification number for rock masses, see e.g. Ref. [20]. The second in situ parameter is the disturbance factor, D, which ranges from 0 to 1, see [2]. For undisturbed rock masses $D = 0$.

Based on these parameters the failure criterion is written as

$$\sigma_1' = \sigma_3' + \sigma_{ci}\left(m_b\frac{\sigma_3'}{\sigma_{ci}} + s\right)^a, \tag{1}$$

where $\sigma_1' \geqslant \sigma_2' \geqslant \sigma_3'$ are the effective principal stresses. In Eq. (1) compression is taken as positive, which is often the case in rock mechanics and geotechnical engineering. Later on in this paper tension will taken as positive and this is denoted by $\sigma_1, \sigma_2, \sigma_3$ without a prime. The empirically determined parameters m_b, s and a are given by [2]

$$m_b = m_i e^{(GSI-100)/(28-14D)}, \tag{2}$$

$$s = e^{(GSI-100)/(9-3D)}, \tag{3}$$

$$a = \tfrac{1}{2} + \tfrac{1}{6}(e^{-GSI/15} - e^{-20/3}). \tag{4}$$

The rock mass modulus of elasticity, E_{rm}, can be estimated from

$$E_{rm} = \frac{1 - D/2}{1 + e^{(75+25D-GSI)/11}} \times 10^5 \text{ MPa} \tag{5}$$

or, if the intact rock modulus, E_i, is known

$$E_{rm} = E_i\left(0.02 + \frac{1 - D/2}{1 + e^{(60+15D-GSI)/11}}\right). \tag{6}$$

taken from Ref. [5]. Examples of Poisson's ratio, v, for rock masses are given in [3].

In the context of finite element derivations, extension and tensile stresses are usually taken as positive. This will be the case in the remainder of this paper. The Hoek–Brown yield criterion is then written as

$$f = \sigma_1 - \sigma_3 - \sigma_{ci}\left(s - m_b\frac{\sigma_1}{\sigma_{ci}}\right)^a = 0, \tag{7}$$

where $\sigma_1 \geqslant \sigma_2 \geqslant \sigma_3$ (without a prime) denotes the effective stresses with tension taken as positive. This means that σ_3 denotes the "largest" compressive stress. A projection of the criterion on the σ_1–σ_3 plane in principal stress space can be seen in Fig. 1. In this depiction the yield surface is a curve with a slope that tends towards infinity as the curve approaches the apex point, $\boldsymbol{\sigma}_t$. At the apex $\sigma_1 = \sigma_2 = \sigma_3 = \sigma_t$, with

$$\sigma_t = s\frac{\sigma_{ci}}{m_b} \tag{8}$$

which is the biaxial tensile strength. The uniaxial compressive strength, σ_c, is shown in Fig. 1 and can be calculated by setting $\sigma_1 = 0$ in Eq. (7)

$$\sigma_c = \sigma_{ci}s^a. \tag{9}$$

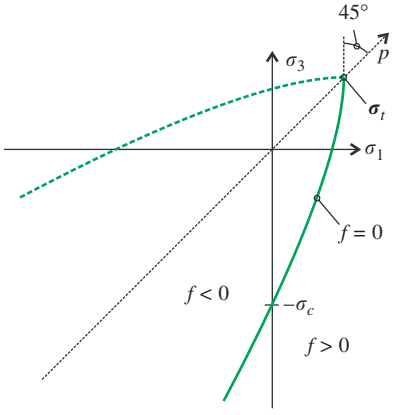

Fig. 1. Projection of the Hoek–Brown criterion on the σ_1–σ_3 plane. The hydrostatic axis is denoted by p. The secondary yield criterion, where $\sigma_3 > \sigma_1$ is shown with a dashed curve.

The trace of the Hoek–Brown yield criterion on the octahedral plane can be seen in Fig. 2. Several cross sections of the criterion corresponding to increasing hydrostatic stress, $p = (\sigma_1 + \sigma_2 + \sigma_3)/3$, have been plotted. It should be noted that the cross sections are not made up of straight lines, but of curves with a very small curvature. The figure shows that as p increases the traces change from an almost regular hexagonal shape into a triangular shape, due to the increasing slope seen in Fig. 1. The octahedral traces have been plotted by expressing the Hoek–Brown criterion, Eq. (7), in stress invariants

$$f = \left(2\sqrt{J_2}\cos\theta\right)^{1/a} - s\sigma_{ci}^{1/a} + m_b\sqrt{J_2}\sigma_{ci}^{1/a-1}\left(\cos\theta - \frac{\sin\theta}{\sqrt{3}}\right) + m_b p\sigma_{ci}^{1/a-1} = 0, \quad (10)$$

where J_2 is the second deviatoric stress invariant and θ is the Lode angle.

The Hoek–Brown criterion in full 3D principal stress space can be seen in Fig. 3. Here it can be seen that the yield surfaces resemble a Mohr–Coulomb pyramid with a curvature. The equations of the five neighbouring yield surfaces can be obtained by interchanging the principal stresses in Eq. (7). In Fig. 4 only the primary yield surface that obeys $\sigma_1 \geqslant \sigma_2 \geqslant \sigma_3$ is shown. The edges of the yield surface are the curves ℓ_1 and ℓ_2, which corresponds to triaxial compression and tension, respectively. The parametric equations of the curves are given by

$$\ell_1: \quad \overline{\boldsymbol{\sigma}} = \begin{Bmatrix} \sigma_1 \\ \sigma_2 \\ \sigma_3 \end{Bmatrix} = \begin{Bmatrix} \sigma_1 \\ \sigma_1 \\ \sigma_1 - \sigma_{ci}\left(s - m_b\dfrac{\sigma_1}{\sigma_{ci}}\right)^a \end{Bmatrix}, \quad (11)$$

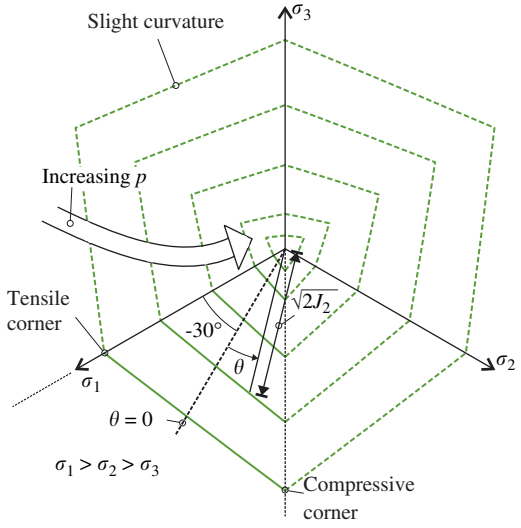

Fig. 2. Several cross sections of the Hoek–Brown criterion on the octahedral plane. Secondary criteria are shown with dotted curves. The geometric interpretations of the Lode angle, θ, and the second deviatoric invariant, J_2, are also shown.

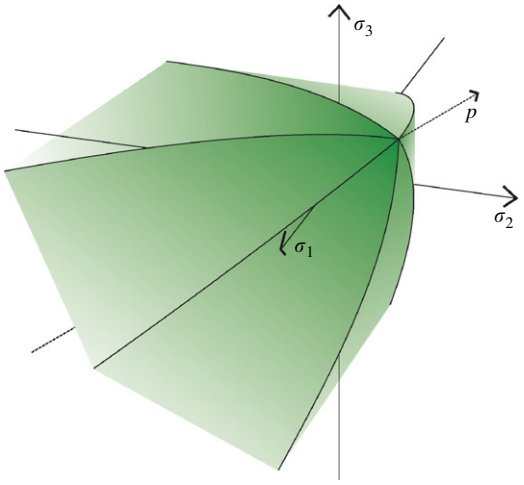

Fig. 3. The Hoek–Brown criterion in principal stress space. The hydrostatic stress axis is denoted by p.

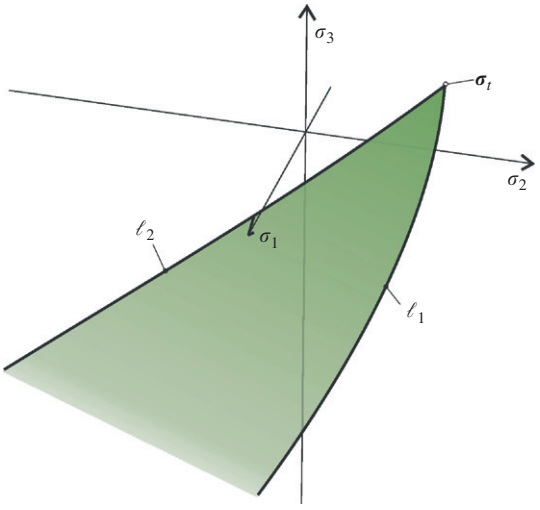

Fig. 4. The primary Hoek–Brown yield surface in principal stress space, i.e. the surface that obeys $\sigma_1 \geqslant \sigma_2 \geqslant \sigma_3$.

$$\ell_2: \quad \overline{\boldsymbol{\sigma}} = \begin{Bmatrix} \sigma_1 \\ \sigma_2 \\ \sigma_3 \end{Bmatrix} = \begin{Bmatrix} \sigma_1 \\ \sigma_1 - \sigma_{ci}\left(s - m_b\dfrac{\sigma_1}{\sigma_{ci}}\right)^a \\ \sigma_1 - \sigma_{ci}\left(s - m_b\dfrac{\sigma_1}{\sigma_{ci}}\right)^a \end{Bmatrix}. \quad (12)$$

2.1. Plastic potential

For non-associated material behaviour a plastic potential resembling the shape of the yield surface is chosen

$$g = \sigma_1 - \sigma_3 - \sigma_{ci}\left(s_g - m_g\frac{\sigma_1}{\sigma_{ci}}\right)^{a_g}. \quad (13)$$

When the parameters of (13) are identical to their yield criterion counterparts, the material behaviour is associated.

2.1.1. Constant rate of dilation

If a constant rate of dilation is required, the curvature parameter a_g should be set to unity, i.e.

$$g_c = g(a_g = 1) = \sigma_1(m_g + 1) - \sigma_3 - \sigma_{ci}s_g. \tag{14}$$

The rate of dilation is then controlled by the parameter m_g.

Computational examples utilising both Eqs. (13) and (14) will be given in Section 11.

3. Elasto-plastic finite element procedure

When the finite element method is used for solving elasto-plastic problems, the load and/or the forced displacement is applied in increments. In each increment equilibrium is sought by minimising the force residual, i.e. the difference between the external and internal forces. Global equilibrium iterations are then carried out until the norm of the residual is smaller than a prescribed number. A popular method for establishing equilibrium is the Newton–Raphson scheme. With the Newton–Raphson scheme the stiffness matrix is updated in each equilibrium iteration. The stresses and the constitutive matrices are updated according to the constitutive law, i.e. linear elastic–perfectly plastic Hoek–Brown plasticity in this paper.

The remainder of this paper deals with the update of the stress and the constitutive matrix.

The stress update can be carried out by different means. The two main classes of stress update is the forward Euler procedure and stress update by return mapping. The basic forward Euler procedure has the advantage of simplicity, which is a notable advantage in the implementation of complex constitutive material models, see e.g. Ref. [21]. One of the drawbacks of the forward Euler procedure is that the updated stress will violate the yield criterion if corrective measures are not taken.

In the recent years it seems that the most used procedure for stress update is the return mapping scheme in some form, which is also the method of choice in this paper. The calculations involved are somewhat more complicated than in the forward Euler method, but an inherent feature of the scheme is that the updated stresses do not violate the yield criterion. The method is also proven to be robust and able to handle reasonably large load steps, see e.g. [18].

Nagtegaal [22] showed that the continuum constitutive matrix, which comes from standard derivations of the elasto-plastic equations and is used in the forward Euler method, is not consistent with a global Newton–Raphson scheme. Simo and Taylor [23] then derived a consistent constitutive matrix for use with the return mapping scheme with global Newton–Raphson iterations. In order to calculate this, the second derivative of the plastic potential, the Hessian matrix, is needed, and this is one of the reasons that the manipulations in the return mapping scheme are more complicated than the basic forward Euler method.

For Hoek–Brown plasticity the direct calculation of the second derivative of the plastic potential is rather cumbersome. Another issue that complicates the implementation of the return mapping scheme for Hoek–Brown plasticity is the presence of discontinuities in the yield surface. Care must be taken in order to ensure a proper stress update and calculation of the constitutive matrix at these points. These discontinuities are the reason that the exact form of Hoek–Brown plasticity has not previously been used in elasto-plastic finite element calculations.

In the following the return mapping method will be summarised followed by the specific formulae for a linear elastic—perfectly plastic Hoek–Brown material.

4. Fundamentals of plasticity and return mapping

The basic relation in small strain plasticity is that a strain increment is composed of an elastic and a plastic part

$$\mathrm{d}\boldsymbol{\varepsilon} = \mathrm{d}\boldsymbol{\varepsilon}^{\mathrm{e}} + \mathrm{d}\boldsymbol{\varepsilon}^{\mathrm{p}}. \tag{15}$$

In perfect plasticity, plastic strains occur during yielding when

$$f(\boldsymbol{\sigma}) = 0 \tag{16a}$$

and

$$\left(\frac{\partial f}{\partial \boldsymbol{\sigma}}\right)^{\mathrm{T}} \mathrm{d}\boldsymbol{\sigma} = 0, \tag{16b}$$

where f is the yield function and $\boldsymbol{\sigma}$ is the stress vector. The matrix transpose is denoted with superscript T. The stress and strain vectors are ordered according to

$$\boldsymbol{\sigma} = [\sigma_x \;\; \sigma_y \;\; \sigma_z \;\; \tau_{xy} \;\; \tau_{xz} \;\; \tau_{yz}]^{\mathrm{T}},$$

$$\boldsymbol{\varepsilon} = [\varepsilon_x \;\; \varepsilon_y \;\; \varepsilon_z \;\; 2\varepsilon_{xy} \;\; 2\varepsilon_{xz} \;\; 2\varepsilon_{yz}]^{\mathrm{T}}. \tag{17}$$

Eq. (16a) describes a closed hypersurface in stress space, and a stress state located inside this surface ($f < 0$) is elastic. As an elastic stress increment is related to an elastic strain increment by Hooke's law, use of Eq. (15) provides

$$\mathrm{d}\boldsymbol{\sigma} = \mathbf{D}\,\mathrm{d}\boldsymbol{\varepsilon}^{\mathrm{e}} = \mathbf{D}(\mathrm{d}\boldsymbol{\varepsilon} - \mathrm{d}\boldsymbol{\varepsilon}^{\mathrm{p}}) = \mathbf{D}\mathrm{d}\boldsymbol{\varepsilon} - \mathbf{D}\,\mathrm{d}\boldsymbol{\varepsilon}^{\mathrm{p}}, \tag{18}$$

where $\mathbf{D}$ is the elastic constitutive matrix given by Young's modulus, E, and Poisson's ratio, v

$$\mathbf{D} = \begin{bmatrix} \overline{\mathbf{D}} & \mathbf{0}_{3\times3} \\ \mathbf{0}_{3\times3} & \overline{\mathbf{G}} \end{bmatrix}, \tag{19}$$

where

$$\overline{\mathbf{D}} = \frac{E}{(1+v)(1-2v)} \begin{bmatrix} 1-v & v & v \\ v & 1-v & v \\ v & v & 1-v \end{bmatrix} \quad \text{and} \tag{20}$$

$$\overline{\mathbf{G}} = \frac{E}{2(1+v)}\mathbf{I}_{3\times3}, \tag{21}$$

where $\mathbf{I}$ is the unit matrix.

For a "finite" strain increment, integration of (18) yields a finite stress increment

$$\Delta\boldsymbol{\sigma} = \mathbf{D}\Delta\boldsymbol{\varepsilon} - \mathbf{D}\Delta\boldsymbol{\varepsilon}^{\mathrm{p}} = \Delta\boldsymbol{\sigma}^{\mathrm{e}} - \Delta\boldsymbol{\sigma}^{\mathrm{p}} \tag{22}$$

which implies the assumption that a finite stress increment is composed of an elastic part followed by a plastic part, see Fig. 5.

Eq. (22) can also be written as

$$\boldsymbol{\sigma}^{\mathrm{C}} = \boldsymbol{\sigma}^{\mathrm{B}} - \Delta\boldsymbol{\sigma}^{\mathrm{p}}. \tag{23}$$

The term $\Delta\boldsymbol{\sigma}^{\mathrm{p}}$ is usually referred to as the plastic corrector stress. The updated stress, $\boldsymbol{\sigma}^{\mathrm{C}}$, and the predictor stress state, $\boldsymbol{\sigma}^{\mathrm{B}}$, are given by

$$\boldsymbol{\sigma}^{\mathrm{C}} = \boldsymbol{\sigma}^{\mathrm{A}} + \Delta\boldsymbol{\sigma}, \tag{24}$$

$$\boldsymbol{\sigma}^{\mathrm{B}} = \boldsymbol{\sigma}^{\mathrm{A}} + \Delta\boldsymbol{\sigma}^{\mathrm{e}}, \tag{25}$$

respectively. Eqs. (22) and (23) are basically the return mapping scheme, which is also illustrated in Fig. 5. In general, plastic strain increments are derived from a plastic potential, g, as

$$\mathrm{d}\boldsymbol{\varepsilon}^{\mathrm{p}} = \mathrm{d}\lambda\frac{\partial g}{\partial\boldsymbol{\sigma}}, \tag{26}$$

where λ is a positive multiplier. Eq. (26) is termed the flow rule. If $g = f$ the flow rule is associated. In principle the plastic corrector is found by inserting Eq. (26) into Eq. (18) and integrating

$$\Delta\boldsymbol{\sigma}^{\mathrm{p}} = \int_{\lambda}^{\lambda+\Delta\lambda}\mathbf{D}\frac{\partial g}{\partial\boldsymbol{\sigma}}\,\mathrm{d}\lambda. \tag{27}$$

Eq. (27) is evaluated as

$$\Delta\boldsymbol{\sigma}^{\mathrm{p}} = \Delta\lambda\mathbf{D}\left.\frac{\partial g}{\partial\boldsymbol{\sigma}}\right|_{\mathrm{C}} \quad \text{or} \tag{28}$$

$$\Delta\boldsymbol{\sigma}^{\mathrm{p}} = \Delta\lambda\mathbf{D}\left.\frac{\partial g}{\partial\boldsymbol{\sigma}}\right|_{\mathrm{B}}, \tag{29}$$

where $|_{\mathrm{C}}$ refers to evaluation at the updated stress point, $\boldsymbol{\sigma}^{\mathrm{C}}$, and $|_{\mathrm{B}}$ at the predictor point, $\boldsymbol{\sigma}^{\mathrm{B}}$. Eq. (28) corresponds to fully implicit integration and usually requires an iterative procedure for general yield criteria, as $\boldsymbol{\sigma}^{\mathrm{C}}$ is unknown. For linear criteria and potentials, Eqs. (28) and (29) yield the same result. Eq. (29) is named the radial return after Krieg and Krieg [24] and is exact for linear yield criteria, but in general not as robust as the implicit version.

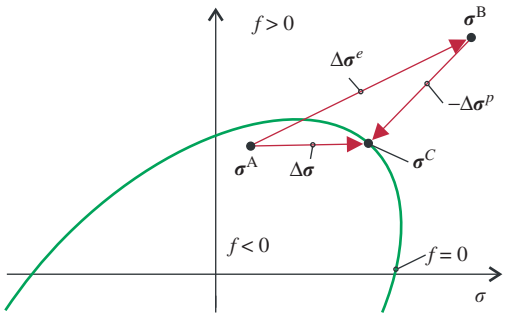

Fig. 5. The principle of return mapping.

5. General and principal stress space

Previous finite element implementations of Hoek–Brown plasticity have carried out the manipulations in the *xyz*-stress space, where the criterion and the plastic potential are expressed via the stress invariants, see Eq. (10). The return mapping scheme requires the first derivative of the yield function and the first and second derivatives of the plastic potential. The expressions for these derivatives are quite complicated in general stress space. Moreover the handling of the discontinuities present at the edges and the apex is difficult in the general stress space, which is the reason for the fact that previous implementations utilise some sort of rounding of the corners and the apex.

The Hoek–Brown criterion in its basic form is expressed in the principal stress space, where it can be visualised in three dimensions. Moreover the first and second derivatives of the criterion and the plastic potential are easily computed. These arguments are the motivation behind the method used in the present paper, which is based on performing all the manipulations in the principal stress space. In a return mapping context this path has been taken before for other criteria in e.g. Ref. [25,26], which both rely on complicated tensor algebra. Here a much simpler approach will be taken, which only involves simple matrix manipulations and geometric arguments, along the same lines as Ref. [27].

As the elasto-plastic Hoek–Brown material model is considered isotropic the stress return and calculation of the constitutive matrix can be carried out with respect to any set of coordinate axes. Therefore the predictor stress is transformed into principal stress space and returned to the yield surface. The point is that the principal stress directions do not change during the return stress increment due to the fact that the shear stresses remain zero during the return. This is, however, only true for isotropic materials. The updated stress can then be transformed back into the original co-ordinate system. The constitutive matrices are also formed in principal stress space and then subsequently transformed. All transformations rely on standard coordinate transformation. It will be shown in the following that this approach simplifies the manipulations of Section 4 remarkably. There are two reasons for this. Firstly the dimension of the problem reduces from six to three, and secondly, in the 3D stress space the stress states can be visualised graphically, making it possible to apply geometric arguments.

In the following the stress update is outlined in parts. The first explains how to calculate the updated stress, $\overline{\boldsymbol{\sigma}}^{\mathrm{C}}$, in principal stress space. The second part outlines how to choose the correct form of return and finally the formula for the consistent constitutive matrix will be given.

In this paper a vector or a matrix with an overbar, e.g. $\overline{\mathbf{a}}$ or $\overline{\mathbf{T}}$ has 3 or 3×3 elements expressed with respect to the principal co-ordinate system.

6. Stress update for Hoek–Brown plasticity

From the solution of the global finite element equations, the predictor stress state in the general stress space, $\boldsymbol{\sigma}^{\mathrm{B}}$, is given via Eq. (25). The principal predictor stresses, $\overline{\boldsymbol{\sigma}}^{\mathrm{B}}$, are then found by standard methods. In principal stress space the stress is then returned to the yield surface and the updated stress is then back transformed into xyz-space.

For Hoek–Brown plasticity four different stress returns apply, as can be seen in Fig. 6:

- return to the yield surface;
- return to the curve ℓ_1;
- return to the curve ℓ_2;
- return to the apex $\overline{\boldsymbol{\sigma}}_t$.

The method for determining the correct return is outlined in Section 7. The first step is to determine whether the stress should be returned to the apex. If this is the case the updated stress is simply the apex stress defined in Eq. (8). If the stress is not to be returned to the apex, a yield surface return is initiated, which will be outlined in the following.

The method for returning the stress to the edges is outlined in Appendices B and C.

For use in the following the gradients of the yield surface, Eq. (7), and the plastic potential, Eq. (13), will be given here,

$$\overline{\mathbf{a}} = \frac{\partial f}{\partial \overline{\boldsymbol{\sigma}}} = \begin{Bmatrix} k \\ 0 \\ -1 \end{Bmatrix} \tag{30a}$$

and

$$\overline{\mathbf{b}} = \frac{\partial g}{\partial \overline{\boldsymbol{\sigma}}} = \begin{Bmatrix} k_g \\ 0 \\ -1 \end{Bmatrix}, \tag{30b}$$

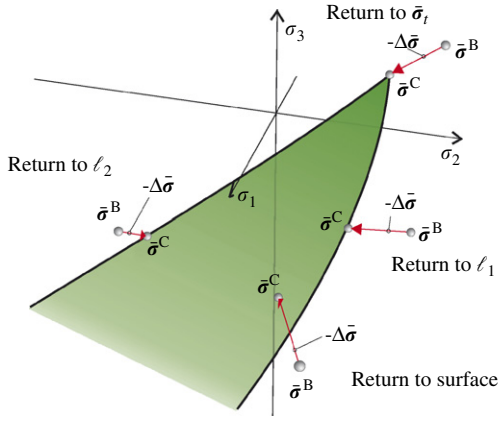

Fig. 6. The four different stress returns.

where k and k_g are the derivatives with respect to σ_1,

$$k = \frac{\partial f}{\partial \sigma_1} = 1 + a m_b \left(s - m_b \frac{\sigma_1}{\sigma_{\mathrm{ci}}} \right)^{a-1} \quad \text{and} \tag{31}$$

$$k_g = \frac{\partial g}{\partial \sigma_1} = 1 + a_g m_g \left(s_g - m_g \frac{\sigma_1}{\sigma_{\mathrm{ci}}} \right)^{a_g - 1}. \tag{32}$$

The gradients $\overline{\mathbf{a}}$ and $\overline{\mathbf{b}}$ can be seen in Fig. 7.

6.1. Return to the yield surface

As the yield surface gradients and plastic potential gradients are always located in the (σ_1, σ_3)-plane, the iterations needed to determine the stress return are 1D only, i.e. a scalar Newton–Raphson procedure is sufficient. The unknowns are the largest and smallest principal stress, σ_1^{C} and σ_3^{C}. These terms are connected according to Eq. (7), which can be rewritten in order to reduce the problem to a single variable

$$\sigma_3(\sigma_1) = \sigma_1 - \sigma_{\mathrm{ci}} \left(s - m_{\mathrm{b}} \frac{\sigma_1}{\sigma_{\mathrm{ci}}} \right)^{a}. \tag{33}$$

The value of the updated intermediate principal stress, σ_2^{C}, can be found from the elastic return calculation, once σ_1^{C} and σ_3^{C} have been determined.

Consider the terms presented in Fig. 7. On the figure a line connects the current updated stress point, $\overline{\boldsymbol{\sigma}}_i^{\mathrm{C}}$, with the stress predictor point $\overline{\boldsymbol{\sigma}}^{\mathrm{B}}$. The direction of the current plastic corrector, $\overline{\mathbf{s}}$, is also shown. From Eqs. (28) and (30), this direction is given by

$$\overline{\mathbf{s}} = \overline{\mathbf{D}}\overline{\mathbf{b}} = \frac{E}{(1+\nu)(1-2\nu)} \begin{Bmatrix} (1-\nu)k_g - \nu \\ \nu k_g - \nu \\ \nu k_g - 1 + \nu \end{Bmatrix} \tag{34}$$

with $\overline{\mathbf{b}}$ given by Eq. (30) and $\overline{\mathbf{D}}$ being the elastic constitutive relation between normal components given by Eq. (20).

The slope of the line connecting $\overline{\boldsymbol{\sigma}}_i^{\mathrm{C}}$ with $\overline{\boldsymbol{\sigma}}^{\mathrm{B}}$ is denoted by α_r. The slope of $\overline{\mathbf{s}}$ is denoted by α_s. For the exact updated stress these slopes must be identical, i.e.

$$h_{\mathrm{f}}(\overline{\boldsymbol{\sigma}}^{\mathrm{C}}) = h_{\mathrm{f}}(\sigma_1^{\mathrm{C}}) = \alpha_r - \alpha_s = 0. \tag{35}$$

The task is then to solve Eq. (35) for σ_1^{C}. This is done efficiently with the Newton–Raphson method. From the current value of the returned largest principal stress, $\sigma_{1,i}^{\mathrm{C}}$, at

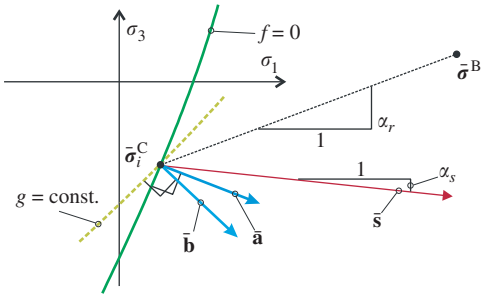

Fig. 7. Return to the yield surface. Projection onto the σ_1–σ_3 plane.

iteration step i, a new estimate is given by

$$\sigma_{1,i+1}^{C} = \sigma_{1,i}^{C} - \frac{h_f(\sigma_{1,i}^{C})}{h_f'(\sigma_{1,i}^{C})}. \tag{36}$$

Iterations are performed until

$$|\sigma_{1,i+1}^{C} - \sigma_{1,i}^{C}| < \mathrm{TOL}, \tag{37}$$

where TOL is the tolerance. The detailed calculation of h_f' can be found in Appendix A.

It should be noted that h_f is not defined for stress values beyond the apex, i.e. if $\sigma_1 > \sigma_t$. In case Eq. (36) yields $\sigma_{1,i+1}^{C} > \sigma_t$ a corrected new estimate can be found by

$$\sigma_{1,i+1}^{C} = \varrho\sigma_t + (1-\varrho)\sigma_{1,i}^{C}, \quad 0 < \varrho < 1, \tag{38}$$

where the authors have found that $\varrho = 0.9$ works well.

When a value of σ_1^{C} that satisfies Eq. (37) is found, σ_3^{C} is found by inserting σ_1^{C} into Eq. (33). The value of the intermediate principal stress is found from Eq. (34) by realising that

$$\Delta\boldsymbol{\sigma}^{p} = t_f \mathbf{s}, \tag{39}$$

where t_f is a scaling factor. The updated value of σ_2^{C} can then be found as

$$\sigma_2^{C} = t_f s_2 + \sigma_2^{B} \quad \text{with } t_f = \frac{\sigma_1^{C} - \sigma_1^{B}}{s_1}, \tag{40}$$

where s_1, s_2 are the first and second elements of $\bar{\mathbf{s}}$, see Eq. (34).

The plastic corrector, which is needed in the calculation of the constitutive matrix in Section 8, is found from Eq. (23) as

$$\Delta\bar{\boldsymbol{\sigma}}^{p} = \bar{\boldsymbol{\sigma}}^{B} - \bar{\boldsymbol{\sigma}}^{C}. \tag{41}$$

7. Determination of correct stress return

This section will clarify which type of stress return should be used.

7.1. Conditions for an apex return

First the concept of boundary planes is introduced in order to determine if the stress should be returned to the apex. A boundary plane is a plane in principal stress space that separates different stress regions. The boundary planes $p_1 = 0$ and $p_2 = 0$, that forms the boundary of the apex return stress region, are shown in Fig. 8 together with their normals, $\bar{\mathbf{n}}_1$ and $\bar{\mathbf{n}}_2$. With the equations of these boundary planes in hand, the conditions for a possible stress return to the apex are

$$f(\bar{\boldsymbol{\sigma}}^{B}) > 0 \ \wedge\ p_1(\bar{\boldsymbol{\sigma}}^{B}) \geqslant 0 \ \wedge\ p_2(\bar{\boldsymbol{\sigma}}^{B}) \geqslant 0. \tag{42}$$

Three direction vectors, $\bar{\mathbf{s}}^{t}, \bar{\mathbf{s}}_1$ and $\bar{\mathbf{s}}_2$, define the orientation of the two planes, see Fig. 8. These vectors are the stress directions corresponding to three unique strain directions

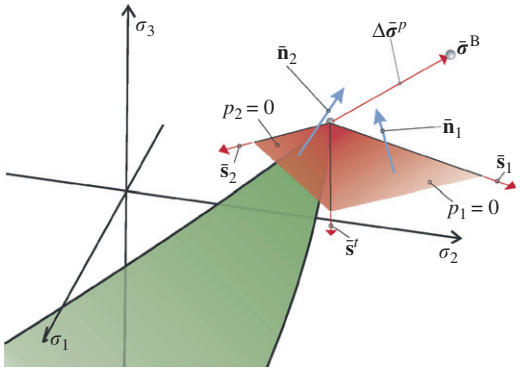

Fig. 8. Boundary planes and their normal vectors for determining whether a predictor stress should be returned to the apex.

at the apex, denoted by $\bar{\mathbf{b}}^{t}$, $\bar{\mathbf{b}}_1$ and $\bar{\mathbf{b}}_2$, i.e.

$$\bar{\mathbf{s}}^{t} = \overline{\mathbf{D}\mathbf{b}}^{t}, \quad \bar{\mathbf{s}}_1 = \overline{\mathbf{D}\mathbf{b}}_1 \quad \text{and} \quad \bar{\mathbf{s}}_2 = \overline{\mathbf{D}\mathbf{b}}_2. \tag{43}$$

The first of the strain directions is the plastic potential normal at the apex, $\bar{\mathbf{b}}^{t}$, which from Eq. (30b) is found as

$$\bar{\mathbf{b}}^{t} = [k_g(\sigma_t) \ \ 0 \ \ -1]^{T}. \tag{44}$$

If $k_g(\sigma_t) = \infty$, which is the case for associated plasticity, $\bar{\mathbf{b}}^{t}$ is evaluated as

$$\bar{\mathbf{b}}^{t} = [1 \ \ 0 \ \ 0]^{T}. \tag{45}$$

The second direction is the strain direction at the apex, $\bar{\mathbf{b}}_1$, parallel to the compressive plane $\sigma_1 = \sigma_2$, i.e.

$$\bar{\mathbf{b}}_1 = \left[1 \ \ 1 \ \ \frac{-2}{k_g(\sigma_t)}\right]^{T}, \tag{46}$$

where the fact that $\bar{\mathbf{b}}_1$ is perpendicular to the direction of the potential line, $\bar{\mathbf{r}}_1^{g}$, Eq. (B.2), has been exploited. Analogously the third strain direction, $\bar{\mathbf{b}}_2$ parallel to the tensile plane, $\sigma_2 = \sigma_3$ is found as

$$\bar{\mathbf{b}}_2 = \left[-2 \quad \frac{1}{k_g(\sigma_t)} \quad \frac{1}{k_g(\sigma_t)}\right]^{T}. \tag{47}$$

As stated earlier, the stress directions $\bar{\mathbf{s}}^{t}$, $\bar{\mathbf{s}}_1$ and $\bar{\mathbf{s}}_2$ define the orientation of the boundary plane normals, which are also shown in Fig. 8. The normals $\bar{\mathbf{n}}_1$ and $\bar{\mathbf{n}}_2$ are calculated by

$$\bar{\mathbf{n}}_1 = \bar{\mathbf{s}}^{t} \times \bar{\mathbf{s}}_1 \quad \text{and} \quad \bar{\mathbf{n}}_2 = \bar{\mathbf{s}}_2 \times \bar{\mathbf{s}}^{t}. \tag{48}$$

Finally the equation of the boundary planes are given as

$$p_1(\bar{\boldsymbol{\sigma}}) = \bar{\mathbf{n}}_1^{T}(\bar{\boldsymbol{\sigma}} - \bar{\boldsymbol{\sigma}}_t) = 0 \quad \text{and} \tag{49}$$

$$p_2(\bar{\boldsymbol{\sigma}}) = \bar{\mathbf{n}}_2^{T}(\bar{\boldsymbol{\sigma}} - \bar{\boldsymbol{\sigma}}_t) = 0, \tag{50}$$

where $\bar{\boldsymbol{\sigma}} = \bar{\boldsymbol{\sigma}}^{B}$ when the predictor stress state is evaluated using Eq. (42).

7.2. Conditions for surface or line returns

If the stress is not to be returned to the apex point, i.e. the conditions in Eq. (42) are not fulfilled, a surface return is carried out as outlined in Section 6.1 and $\bar{\boldsymbol{\sigma}}^{C} =$

$[\sigma_1^C \ \sigma_2^C \ \sigma_3^C]^T$ is calculated. The components of $\overline{\boldsymbol{\sigma}}^C$ reveal if the yield surface return is correct:

- If $\sigma_1^C \geqslant \sigma_2^C \geqslant \sigma_3^C$ then the return to the yield surface is correct.
- If $\sigma_2^C \geqslant \sigma_1^C$ then the stress must be returned to the curve ℓ_1 with the procedure outlined in Appendix B.
- If $\sigma_2^C \leqslant \sigma_3^C$ then the stress must be returned to the curve ℓ_2 with the procedure outlined in Appendix C.

When the stress is returned to a curve, an efficient first estimate of $\sigma_{1,i=1}^C$ in the iteration procedure is the former value of σ_1^C from the yield surface return.

8. Consistent constitutive matrix for the Hoek–Brown criterion

In general stress space the constitutive matrix consistent with the global Newton scheme for the global equilibrium equations, $\mathbf{D}^{epc}$, is given by

$$\mathbf{D}^{epc} = \mathbf{D}^c - \frac{\mathbf{D}^c(\partial g/\partial \boldsymbol{\sigma})(\partial f/\partial \boldsymbol{\sigma})^T \mathbf{D}^c}{(\partial f/\partial \boldsymbol{\sigma})^T \mathbf{D}^c \partial g/\partial \boldsymbol{\sigma}}, \tag{51}$$

where $\mathbf{D}^c$ is a modified elastic stiffness given by

$$\mathbf{D}^c = \mathbf{T}\mathbf{D}. \tag{52}$$

The modification matrix, $\mathbf{T}$, is given by

$$\mathbf{T} = \left(\mathbf{I} + \Delta\lambda \mathbf{D} \frac{\partial^2 g}{\partial \boldsymbol{\sigma}^2}\right)^{-1}, \tag{53}$$

where all the terms are evaluated at the updated stress point, $\boldsymbol{\sigma}^C$. The derivation of $\mathbf{D}^{epc}$ can be found in e.g. [18].

This formulation of $\mathbf{D}^{epc}$ is valid for a return to a yield surface. In this section it will be shown that the calculation of the consistent constitutive matrix in principal stress space, $\hat{\mathbf{D}}^{epc}$, is a simple task compared to a direct calculation in general stress space using Eqs. (53), (52) and (51). In this section a vector or a matrix with a hat, "$\hat{\bullet}$" is a full 6×1 vector or 6×6 matrix expressed with respect to the principal coordinate axes. This is as opposed to the overbar "$\overline{\bullet}$" introduced in Section 5, which signifies a 3×1 vector and a 3×3 matrix relating to the normal components only.

The calculation of $\hat{\mathbf{D}}^{epc}$ is dependent on whether the returned stress belongs to the yield surface, a line or a point. In the following formulae for $\hat{\mathbf{D}}^{epc}$ for the three cases will be shown.

8.1. Calculation of $\mathbf{D}^{epc}$ on the yield surface

In the evaluation of $\mathbf{T}$ the second derivative of the plastic potential is needed, cf. Eq. (53). A direct calculation of this derivative demands that the potential, (13), must be given in general stress space, where the derivations are a cumbersome task. As will be shown this calculation simplifies when carried out in principal stress space. This is done in two steps. First with respect to the normal stresses, $\overline{\mathbf{T}} = \hat{\mathbf{T}}_{1-3,1-3}$, and then with respect to the shear stress related part of $\hat{\mathbf{T}}$.

The second derivative in principal stress space with respect to the principal stresses $\partial^2 g/\partial \overline{\boldsymbol{\sigma}}^2$ is simply calculated by differentiation of the potential in Eq. (13)

$$\frac{\partial^2 g}{\partial \overline{\boldsymbol{\sigma}}^2} = \begin{bmatrix} \dfrac{dk_g}{d\sigma_1} & & \\ & 0 & \\ & & 0 \end{bmatrix}, \tag{54}$$

where $dk_g/d\sigma_1 = \partial^2 g/\partial \sigma_1^2$ is given in Eq. (A.5).

Then $\overline{\mathbf{T}}$ is given by

$$\overline{\mathbf{T}} = \left(\underset{3\times 3}{\mathbf{I}} + \Delta\lambda \overline{\mathbf{D}} \frac{\partial^2 g}{\partial \overline{\boldsymbol{\sigma}}^2}\right)^{-1}. \tag{55}$$

The plastic multiplier $\Delta\lambda$ can be found from e.g.

$$\Delta\lambda = \frac{\|\Delta \overline{\boldsymbol{\sigma}}^p\|}{\|\overline{\mathbf{D}}\overline{\mathbf{b}}\|}, \tag{56}$$

where $\overline{\mathbf{b}} = \partial g/\partial \overline{\boldsymbol{\sigma}}$ is the plastic potential normal, given by Eq. (30b) and $\|\bullet\|$ signifies the euclidian norm of the vector.

The lower right 3×3 part of $\hat{\mathbf{T}}$, denoted by $\overline{\mathbf{T}}_G = \hat{\mathbf{T}}_{4-6,4-6}$, relating to the shear stresses assumes a particularly simple form as shown by Clausen et al. [27]

$$\overline{\mathbf{T}}_G = \left(\underset{3\times 3}{\mathbf{I}} + \begin{bmatrix} \dfrac{\Delta\sigma_1^p - \Delta\sigma_2^p}{\sigma_1^C - \sigma_2^C} & & \\ & \dfrac{\Delta\sigma_1^p - \Delta\sigma_3^p}{\sigma_1^C - \sigma_3^C} & \\ & & \dfrac{\Delta\sigma_2^p - \Delta\sigma_3^p}{\sigma_2^C - \sigma_3^C} \end{bmatrix}\right)^{-1}. \tag{57}$$

If any of the denominators in Eq. (57) vanish, the corresponding element in $\overline{\mathbf{T}}_G$ vanishes.

The modification matrix, $\hat{\mathbf{T}}$ for stress return to the yield surface is then assembled as

$$\hat{\mathbf{T}} = \begin{bmatrix} \overline{\mathbf{T}} & \\ & \overline{\mathbf{T}}_G \end{bmatrix}. \tag{58}$$

The consistent constitutive matrix in principal stress space, $\hat{\mathbf{D}}^{epc}$ is then calculated by Eq. (51) by replacing $\mathbf{D}^c$ with $\hat{\mathbf{D}}^c = \hat{\mathbf{T}}\mathbf{D}$,

$$\hat{\mathbf{D}}^{epc} = \hat{\mathbf{D}}^c - \frac{\hat{\mathbf{D}}^c \hat{\mathbf{b}} \hat{\mathbf{a}}^T \hat{\mathbf{D}}^c}{\hat{\mathbf{a}}^T \hat{\mathbf{D}}^c \hat{\mathbf{b}}}, \tag{59}$$

where

$$\hat{\mathbf{a}} = [\overline{\mathbf{a}}^T \ 0 \ 0 \ 0]^T \quad \text{and}$$

$$\hat{\mathbf{b}} = [\overline{\mathbf{b}}^T \ 0 \ 0 \ 0]^T. \tag{60}$$

8.2. Calculation of $\mathbf{D}^{\mathrm{epc}}$ on a curve

When a stress return is made to a curve the modification matrix, $\mathbf{T}$, is changed slightly compared to the yield surface return, see e.g. [18],

$$\mathbf{T}_\ell = \left(\mathbf{I} + \Delta\lambda \mathbf{D}\frac{\partial^2 g}{\partial \boldsymbol{\sigma}^2} + \Delta\lambda_n \mathbf{D}\frac{\partial^2 g_n}{\partial \boldsymbol{\sigma}^2}\right)^{-1}, \tag{61}$$

where $\Delta\lambda_n$ is the plastic multiplier related to the neighbouring plastic potential, g_n. Two neighbour plastic potentials, namely the compressive neighbour potential and the tensile neighbour potential will be used. The corresponding yield surfaces are shown in Fig. 9. The equations of the neighbour potentials and their derivatives are obtained by interchanging the components of the principal stress vector as shown in Fig. 9. For the compressive secondary region with $\sigma_2 > \sigma_1 > \sigma_3$ the terms needed in calculating $\hat{\mathbf{T}}$ are

$$\overline{\mathbf{b}}_n = \frac{\partial g_n}{\partial \overline{\boldsymbol{\sigma}}} = \begin{Bmatrix} 0 \\ k_g \\ -1 \end{Bmatrix}, \quad \frac{\partial^2 g_n}{\partial \overline{\boldsymbol{\sigma}}^2} = \begin{bmatrix} 0 & & \\ & \dfrac{\mathrm{d}k_g}{\mathrm{d}\sigma_1} & \\ & & 0 \end{bmatrix}, \tag{62}$$

where it should be noted that $\sigma_1 = \sigma_2$ when returning to ℓ_1 and therefore $\mathrm{d}k_g/\mathrm{d}\sigma_2 = \mathrm{d}k_g/\mathrm{d}\sigma_1$. See Eqs. (32) and (A.5) for k_g and $\mathrm{d}k_g/\mathrm{d}\sigma_2$.

For a return to the tensile corner, i.e. the curve ℓ_2, the terms needed are

$$\overline{\mathbf{b}}_n = \frac{\partial g_n}{\partial \overline{\boldsymbol{\sigma}}} = \begin{Bmatrix} k_g \\ -1 \\ 0 \end{Bmatrix}, \quad \frac{\partial^2 g_n}{\partial \overline{\boldsymbol{\sigma}}^2} = \begin{bmatrix} \dfrac{\mathrm{d}k_g}{\mathrm{d}\sigma_1} & & \\ & 0 & \\ & & 0 \end{bmatrix}. \tag{63}$$

8.2.1. Plastic multipliers

When returning to a curve, the assumption by Koiter [28] states that the plastic strain is a linear combination of the strain directions involved,

$$\Delta\overline{\boldsymbol{\varepsilon}}^{\mathrm{p}} = \Delta\lambda\overline{\mathbf{b}} + \Delta\lambda_n\overline{\mathbf{b}}_n, \tag{64}$$

where $\Delta\overline{\boldsymbol{\varepsilon}}^{\mathrm{p}} = \overline{\mathbf{D}}^{-1}\Delta\overline{\boldsymbol{\sigma}}^{\mathrm{p}}$, see Eq. (B.4).

For the compressive corner, ℓ_1, this gives

$$\Delta\overline{\boldsymbol{\varepsilon}}^{\mathrm{p}} = \begin{Bmatrix} \Delta\varepsilon_1^{\mathrm{p}} \\ \Delta\varepsilon_2^{\mathrm{p}} \\ \Delta\varepsilon_3^{\mathrm{p}} \end{Bmatrix} = \Delta\lambda \begin{Bmatrix} k_g \\ 0 \\ -1 \end{Bmatrix} + \Delta\lambda_n \begin{Bmatrix} 0 \\ k_g \\ -1 \end{Bmatrix} \tag{65}$$

$$\Rightarrow \Delta\lambda = \frac{\Delta\varepsilon_1^{\mathrm{p}}}{k_g} \quad \text{and} \quad \Delta\lambda_n = \frac{\Delta\varepsilon_2^{\mathrm{p}}}{k_g}. \tag{66}$$

For the tensile corner, ℓ_2, we have

$$\Delta\overline{\boldsymbol{\varepsilon}}^{\mathrm{p}} = \begin{Bmatrix} \Delta\varepsilon_1^{\mathrm{p}} \\ \Delta\varepsilon_2^{\mathrm{p}} \\ \Delta\varepsilon_3^{\mathrm{p}} \end{Bmatrix} = \Delta\lambda \begin{Bmatrix} k_g \\ 0 \\ -1 \end{Bmatrix} + \Delta\lambda_n \begin{Bmatrix} k_g \\ -1 \\ 0 \end{Bmatrix} \tag{67}$$

$$\Rightarrow \Delta\lambda = -\Delta\varepsilon_3^{\mathrm{p}} \quad \text{and} \quad \Delta\lambda_n = -\Delta\varepsilon_2^{\mathrm{p}}. \tag{68}$$

Now $\overline{\mathbf{T}}$ can be computed from Eq. (61) with insertion of terms for either ℓ_1, Eqs. (54), (62) and (66), or for ℓ_2, Eqs. (54), (63) and (68). The full modification matrix in principal stress space, $\hat{\mathbf{T}}$ is again given by Eq. (58), as the shear components $\overline{\mathbf{T}}_G$ are still given by Eq. (57) when the returned stress is on an edge curve.

8.2.2. Constitutive matrix on a curve

With the modification matrix at hand, the modified elastic stiffness matrix in principal stress space, $\hat{\mathbf{D}}^{\mathrm{c}}$ is then given by Eq. (52), $\hat{\mathbf{D}}^{\mathrm{c}} = \hat{\mathbf{T}}\mathbf{D}$.

On a yield surface the consistent constitutive matrix, $\hat{\mathbf{D}}^{\mathrm{epc}}$, would be calculated by Eq. (59), which shows that $\hat{\mathbf{D}}^{\mathrm{epc}}$ is singular with respect to the plastic potential normal, $\hat{\mathbf{b}}$, i.e.

$$\hat{\mathbf{D}}^{\mathrm{epc}}\hat{\mathbf{b}} = \underset{6\times 1}{\mathbf{0}}. \tag{69}$$

When the stress state is located on a curve, $\hat{\mathbf{D}}^{\mathrm{epc}}$ must be singular with respect to *all* directions perpendicular to the direction vector of the plastic potential curve, $\overline{\mathbf{r}}^g$. In principal stress space the consistent constitutive matrix that fulfils this condition is given by [29]

$$\hat{\mathbf{D}}^{\mathrm{epc}} = \begin{bmatrix} \dfrac{\overline{\mathbf{r}}(\overline{\mathbf{r}}^g)^{\mathrm{T}}}{(\overline{\mathbf{r}})^{\mathrm{T}}(\overline{\mathbf{D}}^{\mathrm{c}})^{-1}\overline{\mathbf{r}}^g} & \\ & \overline{\mathbf{G}}^{\mathrm{c}} \end{bmatrix}, \tag{70}$$

where $\overline{\mathbf{G}}^{\mathrm{c}}$ is the bottom right 3×3 quadrant of $\hat{\mathbf{D}}^{\mathrm{c}}$, i.e. is the modified elastic equivalent of $\overline{\mathbf{G}}$ defined in Eq. (21). The formula for the double singular constitutive matrix of Eq. (70) is a great simplification compared to the expression for a double singular constitutive matrix in general stress space, see e.g. Ref. [18].

8.2.3. Constitutive matrix on the apex

When the updated stress is located on the apex the constitutive matrix must be singular with respect to all the

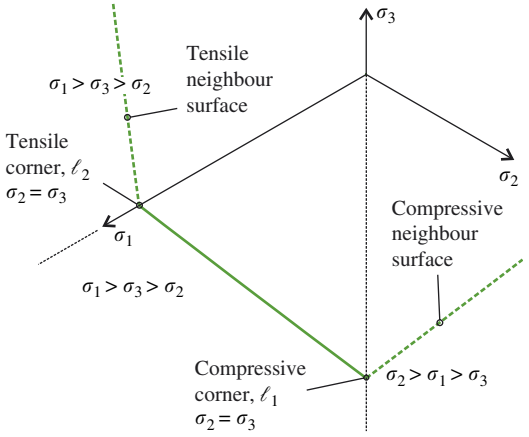

Fig. 9. A cross section of the Hoek–Brown criterion on the octahedral plane. Compressive and tensile neighbour criteria are shown with dashed curves.

intersecting yield surfaces. This means that it must be a zero matrix, i.e.

$$\mathbf{D}^{\mathrm{epc}} = \underset{6\times 6}{\mathbf{0}}. \tag{71}$$

If many stress points are located at the apex this can lead to a singular global stiffness matrix. However, in almost any practical problem most points in the calculation domain will be in a state of compression, and the formulation of Eq. (71) causes no difficulties. If, for some reason, a considerable amount of stress points is located at the apex there are ways to deal with this, see Ref. [30].

9. Summary of the method

A summary of the method can be seen in Table 1.

The references in the table refer to a full 3D stress state calculation. It should be noted that 2D calculations differ in some aspects. These differences are explained in Refs. [29,30].

Table 1
Return mapping scheme for the Hoek–Brown criterion. Performed in each Gauss-point

INPUT: $\boldsymbol{\sigma}^{\mathrm{A}}, \Delta\boldsymbol{\varepsilon}, \mathbf{D}$, material parameters

1. $\boldsymbol{\sigma}^{\mathrm{B}} = \boldsymbol{\sigma}^{\mathrm{A}} + \mathbf{D}\Delta\boldsymbol{\varepsilon}$
2. Transform predictor stress, $\boldsymbol{\sigma}^{\mathrm{B}}$, into principal stress space
   $\hat{\boldsymbol{\sigma}}^{\mathrm{B}} = [(\bar{\boldsymbol{\sigma}}^{\mathrm{B}})^{\mathrm{T}}\ 0\ 0\ 0]^{\mathrm{T}}$
3. **Check yield criterion**:
   IF $f(\bar{\boldsymbol{\sigma}}^{\mathrm{B}}) \leqslant 0$: No stress return:
   $\boldsymbol{\sigma}^{\mathrm{C}} = \boldsymbol{\sigma}^{\mathrm{B}}, \quad \mathbf{D}^{\mathrm{epc}} = \mathbf{D}, \quad \Delta\boldsymbol{\varepsilon}^{\mathrm{p}} = \mathbf{0}$
   ELSE Stress return
4. **Stress return and constitutive matrix**
   Compute $p_1(\bar{\boldsymbol{\sigma}}^{\mathrm{B}})$ and $p_2(\bar{\boldsymbol{\sigma}}^{\mathrm{B}})$ from Eq. (42)
   IF $p_1(\bar{\boldsymbol{\sigma}}^{\mathrm{B}}) \geqslant 0 \wedge p_1(\bar{\boldsymbol{\sigma}}^{\mathrm{B}}) \geqslant 0$ return to apex:
   Set $\bar{\boldsymbol{\sigma}}^{\mathrm{C}} = \bar{\boldsymbol{\sigma}}_t$
   Set $\hat{\mathbf{D}}^{\mathrm{epc}} = \underset{6\times 6}{\mathbf{0}}$ from Eq. (71)
   ELSE return to the yield surface:
   Compute $\bar{\boldsymbol{\sigma}}^{\mathrm{C}}$ and $\Delta\bar{\boldsymbol{\sigma}}^{\mathrm{p}}$ by solving Eq. (35)
   Compute $\hat{\mathbf{T}}$ by Eq. (58)
   Compute $\hat{\mathbf{D}}^{\mathrm{epc}}$ by Eqs. (52) and (59)
   END IF
   IF $\sigma_2^{\mathrm{C}} \geqslant \sigma_1^{\mathrm{C}}$ return to curve ℓ_1:
   Compute $\bar{\boldsymbol{\sigma}}^{\mathrm{C}}$ and $\Delta\bar{\boldsymbol{\sigma}}^{\mathrm{p}}$ by solving Eq. (B.3)
   Compute $\hat{\mathbf{T}}$ by Eqs. (61) and (58)
   Compute $\hat{\mathbf{D}}^{\mathrm{epc}}$ by Eqs. (52) and (70)
   ELSE IF $\sigma_2^{\mathrm{C}} \leqslant \sigma_3^{\mathrm{C}}$ return to curve ℓ_2:
   Compute $\bar{\boldsymbol{\sigma}}^{\mathrm{C}}$ and $\Delta\bar{\boldsymbol{\sigma}}^{\mathrm{p}}$ by solving Eq. (B.3)
   Compute $\hat{\mathbf{T}}$ by Eqs. (61) and (58)
   Compute $\hat{\mathbf{D}}^{\mathrm{epc}}$ byEqs. (52) and (70)
   END IF
   $\Delta\bar{\boldsymbol{\varepsilon}}^{\mathrm{p}} = \bar{\mathbf{D}}^{-1}\Delta\bar{\boldsymbol{\sigma}}^{\mathrm{p}}$
5. **Transformation back into the original coordinate system**
   Calculate transformation matrix $\mathbf{A}$, see e.g. Refs. [31,27,30]
   $\boldsymbol{\sigma}^{\mathrm{C}} = \mathbf{A}^{\mathrm{T}}\hat{\boldsymbol{\sigma}}^{\mathrm{C}}$
   $\Delta\boldsymbol{\varepsilon}^{\mathrm{p}} = \mathbf{A}^{-1}\Delta\hat{\boldsymbol{\varepsilon}}^{\mathrm{p}}$
   $\mathbf{D}^{\mathrm{epc}} = \mathbf{A}\hat{\mathbf{D}}^{\mathrm{epc}}\mathbf{A}^{\mathrm{T}}$
   END IF

OUTPUT: $\boldsymbol{\sigma}^{\mathrm{C}}\ \mathbf{D}^{\mathrm{epc}}\ \Delta\boldsymbol{\varepsilon}^{\mathrm{p}}$

In Table 1 the calculation of the plastic strain increment is given. This is not necessary for the stress update calculation, but may be needed for the purpose of tracing and plotting the plastic strain.

10. Comparison with the Drucker–Prager corner approximation

A method of bypassing the singularities when the updated stress is located on a corner curve is to calculate the Drucker–Prager constitutive matrix for this particular stress return, see e.g. Refs. [17,18]. Here a numerical example will indicate the advantage of the presented approach over the Drucker–Prager approximation.

The example is analogous to the numerical example in Section 11.2, where the bearing capacity of a footing on a Hoek–Brown material is computed. See this section for material parameters and geometry.

The Drucker–Prager approximation can be seen in Fig. 10, where also the gradients $\bar{\mathbf{b}}_1^{\mathrm{DP}}$ and $\bar{\mathbf{b}}_2^{\mathrm{DP}}$ at the corners are shown. These gradients are calculated from Eqs. (46) and (47), respectively, with σ_1^{C} replacing σ_t,

$$\bar{\mathbf{b}}_1^{\mathrm{DP}} = \begin{Bmatrix} 1 \\ 1 \\ \dfrac{-2}{k_g(\sigma_1^{\mathrm{C}})} \end{Bmatrix} \quad \text{and} \quad \bar{\mathbf{b}}_2^{\mathrm{DP}} = \begin{Bmatrix} -2 \\ 1 \\ \dfrac{1}{k_g(\sigma_1^{\mathrm{C}})} \\ \dfrac{1}{k_g(\sigma_1^{\mathrm{C}})} \end{Bmatrix}. \tag{72}$$

The yield surface normals are calculated analogously with $k(\sigma_1^{\mathrm{C}})$ replacing $k_g(\sigma_1^{\mathrm{C}})$. The constitutive matrices are then found by Eq. (51). Regarding the constitutive matrix on the apex, this is found by using the values of the potential gradient and the yield surface normal at the apex, i.e. Eq. (44).

The numbers of global equilibrium iterations of the methods are compared, using the bearing capacity calculation

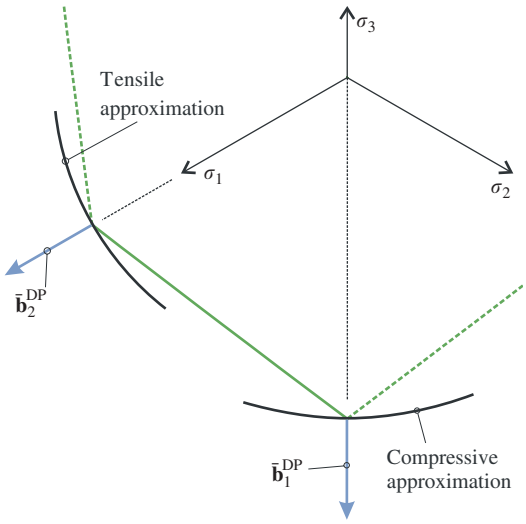

Fig. 10. The Drucker–Prager approximations and potential gradients at the corners.

Table 2
Average numbers of equilibrium iterations for the two methods

	Present method	DP approximation
Plane strain	6.00	9.09
Axisymmetry	5.74	285

of Section 11.2. The material is associated with the parameters of Table 4 and the mesh shown in Fig. 17 is used. A forced displacement is applied in 35 steps. The average numbers of global equilibrium iterations for each load step are shown in Table 2. As seen from the table there is only a small difference for plane strain problems. This is due to the fact that only a few corner and apex returns take place—less than 1% of the total number of returns for this example. In the axisymmetric problem the difference is significant, due to the fact that a large percentage of the stress returns are corner returns, approximately 70% in this example. In this case the present method presents a large improvement. Similar large improvements may be expected in 3D solids.

11. Computational examples

In the following some results from elasto-plastic finite element calculations on a Hoek–Brown material using the presented method will be presented. The elements used are triangular six-noded linear strain elements with two displacement degrees of freedom in each node. Two validation examples and an indication of the consistency of the constitutive matrix will be given.

- Calculation of the displacement of a tunnel wall during excavation.
- The bearing capacity of a strip and circular footing.
- An indication of the efficiency of the presented constitutive matrix is given in Appendix D

The presented method has also been used in an elasto-plastic finite element calculation of the slope safety factor, see Ref. [32].

11.1. Tunnel excavation

A classical axisymmetric problem using a Hoek–Brown material is the calculation of the displacement of tunnel walls during excavation. Several semi-analytical and numerical solutions to this problem exist, see e.g. [6,7,9].

The geometry of the problem is shown in Fig. 11. The excavation of a circular tunnel in an infinite rock mass is simulated by reducing the pressure, p, on the tunnel wall from the initial value p_∞ to the end value $p_0 = 0$. The initial value, p_∞, is the hydrostatic pressure in the infinite rock mass. The tunnel radius is denoted by r_0 and the radius in which the material changes from plastic to elastic behaviour is denoted by R. The displacement of the tunnel wall is denoted u and the final value, u_0, will be compared to the closed form solution, $u_{ex} = 20.9$ mm of [7], as will the value of R, $R_{ex} = 10.62$ m.

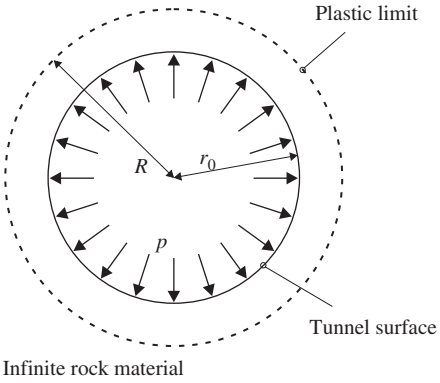

Fig. 11. Geometry and definitions of the tunnel excavation problem.

Table 3
Parameters in the tunnel excavation example

$\sigma_{ci} = 210$ MPa	$E = 60.0$ GPa	$p_\infty = 100.0$ MPa
$m_b = 1.70$	$\nu = 0.20$	$p_0 = 0$
$s = 0.296$	$m_g = 0$	$r_0 = 10.0$ m
$a = 1/2$	$s_g = 0.296$	$u_{ex} = 20.9$ mm
	$a_g = 1$	$R_{ex} = 10.62$ m

The exact solutions, u_{ex} and R_{ex} are taken from Ref. [7].

The material and geometric parameters can be seen in Table 3. From the table it is seen that $a = \frac{1}{2}$, which is the value used in the original Hoek–Brown criterion from Ref. [1]. The curvature parameter of the plastic potential is set to unity, $a_g = 1$, which indicates a constant plastic dilation rate. The value $m_g = 0$ indicates that no plastic dilation takes place, cf. Eq. (14). This is also the case in the closed form solution of Ref. [7].

As the domain boundaries in the problem are infinite, two different finite element boundary conditions will be applied. The first boundary condition will give an upper value of the final wall displacement, $u_0 > u_{ex}$. This is achieved by applying the far-field pressure, p_∞ on the far-field boundary, see Fig. 12a. The second boundary condition gives a lower value of u_0, i.e $u_0 < u_{ex}$. This is achieved by applying a zero radial displacement condition on the far-field boundary, see Fig. 12b. To examine the significance of the extent of the element mesh, different element meshes with varying radial extent, r_{mesh}, have been used. The extent varies between $r_{mesh} = 15$ m and 105 m. And example of an element mesh with $r_{mesh} = 15$ m is shown in Fig. 12c. This particular mesh is made up of 107 elements with a total of 500 degrees of freedom. In the calculations the pressure is reduced from p_∞ to $p_0 = 0$ in nine steps.

In Fig. 13 an example of the displacement–pressure curve can be seen for $r_{mesh} = 40$ m. As expected the upper and lower value solutions are too large and too small, respectively. The average of the two solutions is also shown

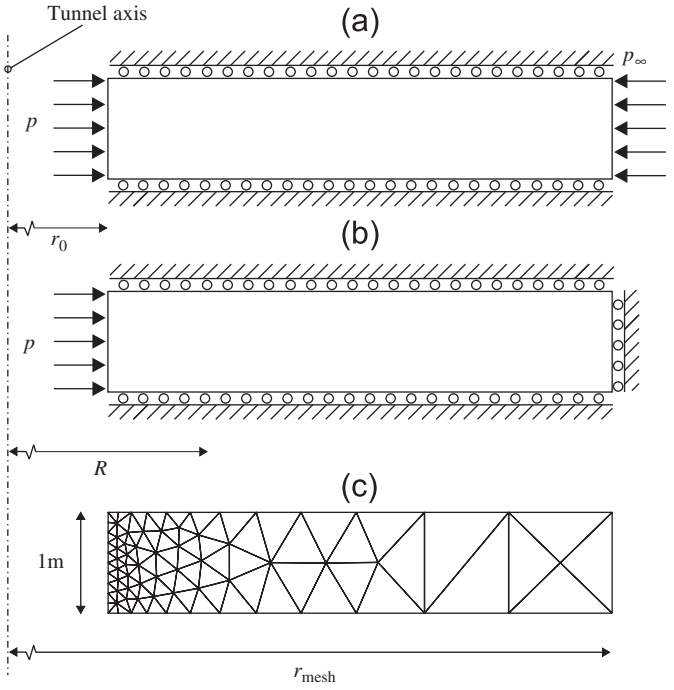

Fig. 12. Example of mesh geometry and boundary conditions. (a) Upper value boundary conditions. (b) Lower value boundary conditions. (c) Example of element mesh with the radius $r_{mesh} = 15$ m. The geometry is axisymmetric around the tunnel axis.

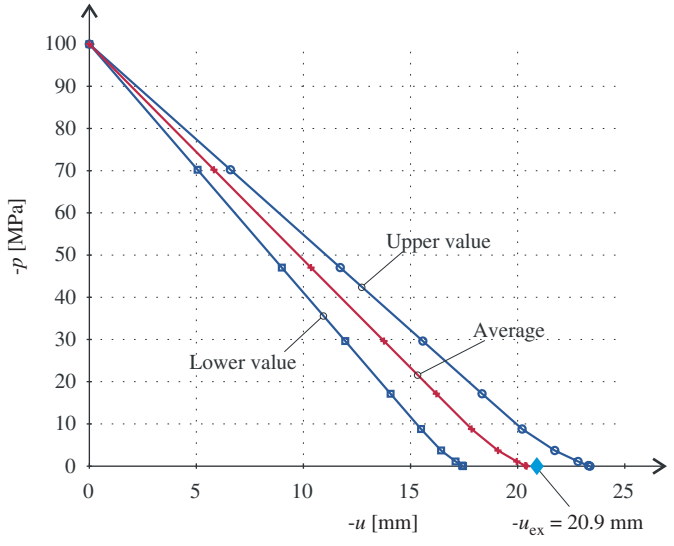

Fig. 13. Example of load–displacement curve for the tunnel wall. The upper value and lower value curves are shown together with their average. The maximum radius of the mesh is $r_{mesh} = 40$ m.

in the figure, and this is fairly close to the exact solution. The curves are straight until the last few steps, which suggests an elastic response until the tunnel wall pressure, p reaches values of approximately 10 MPa. The dependence of the solutions on the mesh extent, r_{mesh}, is shown in Fig. 14, where the relative difference between FEM and the exact values of the final tunnel wall displacement is

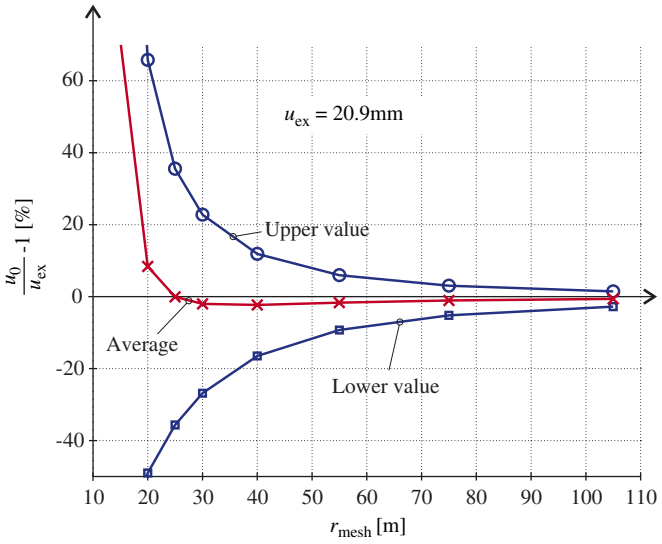

Fig. 14. Final tunnel wall displacement. Difference between finite element and exact solution.

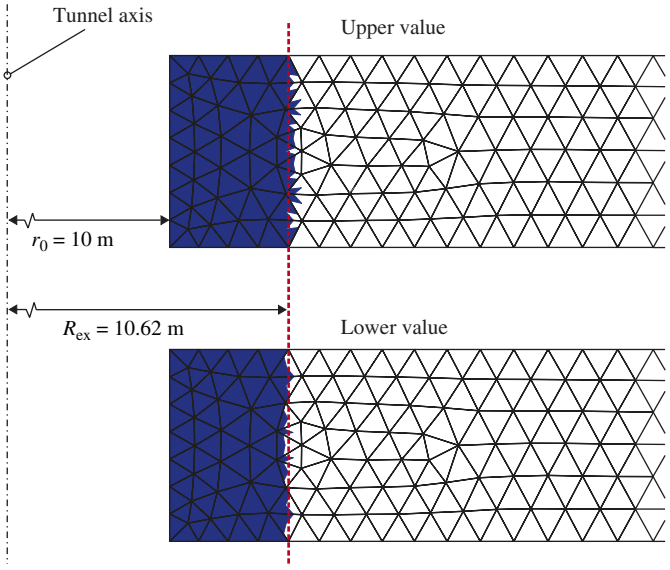

Fig. 15. Yielding elements for the upper and lower value solution compared with the exact solution. The mesh radius is $r_{mesh} = 105$ m.

indicated. As expected the upper and lower bound bracket the exact solution in an interval of decreasing size, as r_{mesh} grows. The average value is also shown. At $r_{mesh} = 105$ m the error on the average value is 0.7%. The extent of the plastic zone can be seen in Fig. 15 for $r_{mesh} = 105$ m. It can be seen that the yielding areas of the finite elements are a good approximation to the exact solution.

11.2. Surface footings on a Hoek–Brown material

The bearing capacity of a footing resting on a Hoek–Brown material has previously been calculated using different approaches, see e.g. the discussion in Ref. [14]. Usually some form of a limit state theorem has been

applied. Here the proposed method will be used for calculating the bearing capacity of both a strip and a circular footing. The result for the strip footing will be compared with the result given by Merifield et al. [14], where a bearing capacity is given as the average of computed upper and lower bound solutions.

The ultimate bearing capacity, q_u, is expressed using the bearing capacity factor, N_σ, and the rock mass compressive strength, σ_{ci},

$$q_u = \sigma_{ci} N_\sigma \tag{73}$$

The value N_σ depends on the other material parameters.

The finite element calculations are carried out with both an associated and a non-associated material. For the non-associated material the value $m_g^{na} = m_b/4$ has been chosen based on the guidelines found in Ref. [33]. The remaining parameters in the plastic potential are equal to their yield criterion counterparts.

The material parameters are chosen to be fairly consistent with a sandstone with $GSI = 30$, $m_i = 17$, $\sigma_{ci} = 75\,\text{MPa}$ and a selfweight $\gamma = 20\,\text{kN/m}^3$. The model parameters are then found Eqs. (2)–(5), where the rock mass is taken to be undisturbed, i.e. $D = 0$. The parameters can be seen in Table 4. The domain geometry and boundary conditions can be seen in Fig. 16. The footing has a halfwidth/radius of $r = 1\,\text{m}$ and the modelled domain has a width and height of 12 and 10 m, respectively. Forced displacement increments are applied to the footing nodes and the footing pressure is calculated as the sum of vertical footing node reactions divided by the footing area.

Table 4
Parameters in the surface footing example

$\sigma_{ci} = 75\,\text{MPa}$	$m_g^{as} = 1.395$	$E = 1644.9\,\text{MPa}$
$m_b = 1.395$	$m_g^{na} = 0.349$	$\nu = 0.30$
$s = 0.0004$	$s_g = 0.0004$	$\gamma = 20\,\text{kN/m}^3$
$a = 0.522$	$a_g = 0.522$	$N_\sigma^{ex} = 0.69$

The comparative solution, N_σ^{ex}, is taken from Ref. [14].

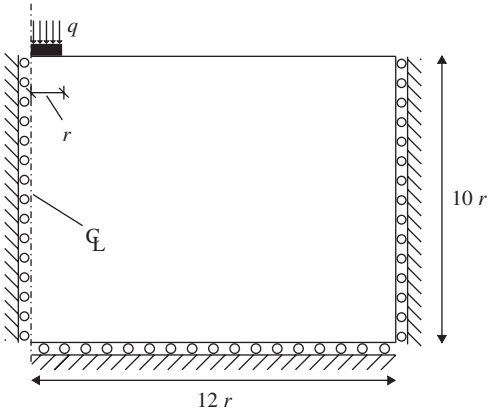

Fig. 16. Geometry and boundary conditions for the footing problem. The domain is symmetric and axisymmetric around the centreline for the plane strain and the axisymmetric example, respectively.

To simulate a rough footing the footing nodes are fixed in the horizontal direction. The domain is meshed with an increasing element density in order to examine the convergence properties of the finite element solution. An example of the element mesh is seen in Fig. 17.

11.2.1. Strip footing

An example of the displacement–load curves for an associated and a non-associated material can be seen in Fig. 18. The example is taken from a calculation with an element mesh with 4684 degrees of freedom. The limit state solution of Merifield et al. [14], $N_\sigma^{ex} = 0.69$, is also shown. It is seen that the displacement–load curves reach a plateau close to the limit state solution, with the bearing capacity of the non-associated material being a bit lower than that of the associated material. The final value of q/σ_{ci} is taken to represent the bearing capacity factor, N_σ. The computed N_σ values for the different element meshes are shown in Fig. 19 versus the number of degrees of freedom. The computed values of N_σ drops as the element mesh is

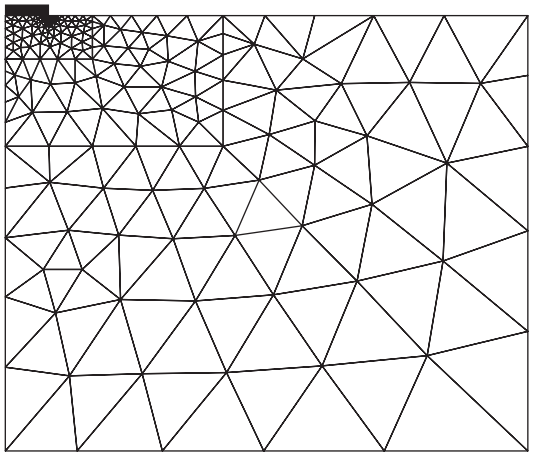

Fig. 17. An example of the element mesh with 347 elements and 1500 degrees of freedom.

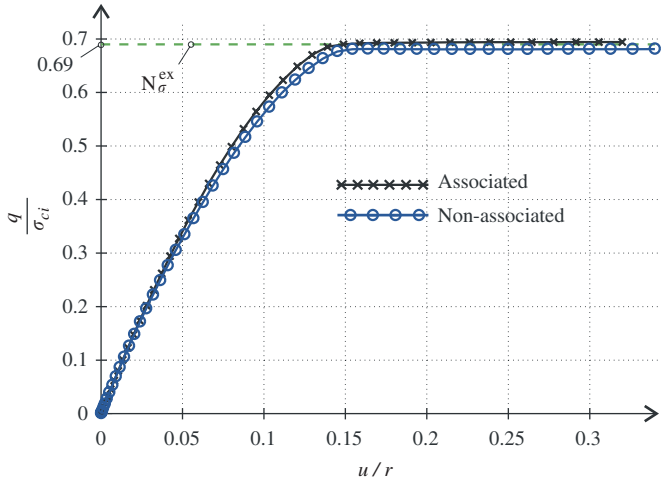

Fig. 18. Example of the normalised displacement–load curves for the strip footing. Calculated using an element mesh with $n_{dof} = 4684$.

refined. This fits well with the fact that the elements are displacement based, and therefore ought to predict a bearing capacity larger than the exact value. The non-associated material model predicts a somewhat lower bearing capacity than the associated one. The lowest bearing capacity factors are $N_\sigma = 0.688$ and 0.677 for the associated and the non-associated material, respectively. For the associated material this is a deviation of -0.26% from the limit state solution.

In order to estimate a convergence value N_σ is plotted against the value h in Fig. 20, see. e.g. [31], given by

$$h = \frac{1}{\sqrt{n_{\text{dof}}}}. \tag{74}$$

A second order polynomial is fitted to the values by the least squares method and interpolated to $h = 0$, which indicates the convergence value. It is seen that the convergence estimates are $N_\sigma^\infty = 0.687$ and 0.668 for the associated and the non-associated material, respectively. The limit state solution is an average between the upper

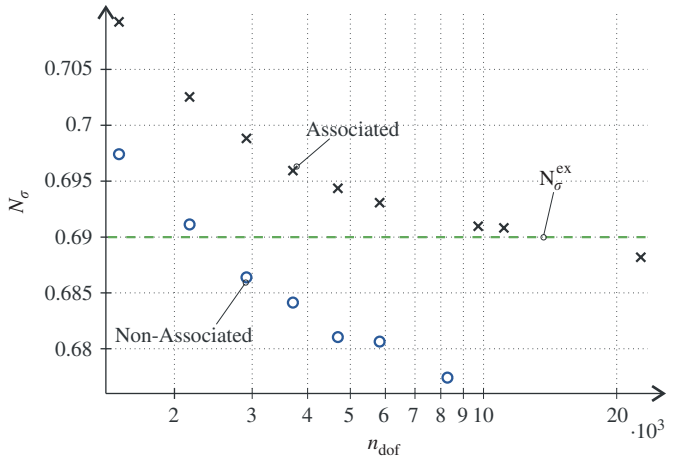

Fig. 19. Calculated N_σ values in plane strain versus the number of degrees of freedom, n_{dof} for the strip footing.

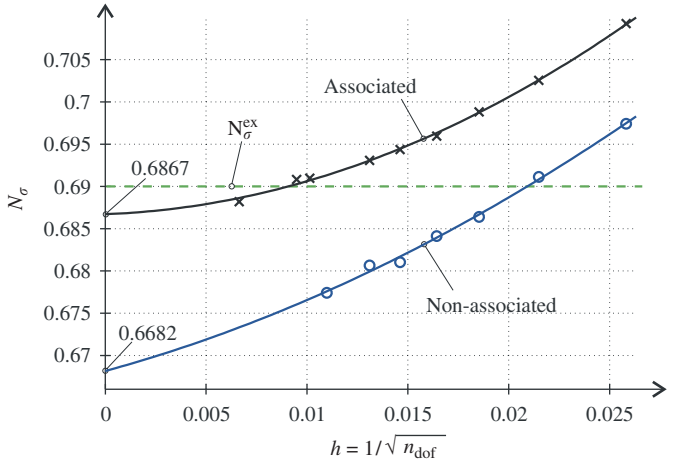

Fig. 20. Curve fitting and convergence for N_σ in plane strain.

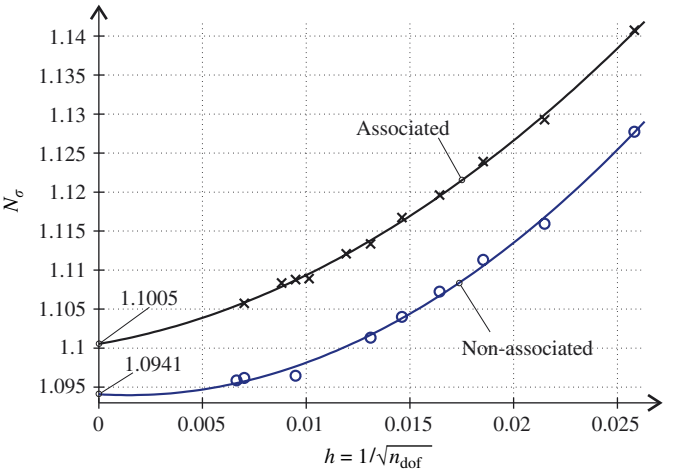

Fig. 21. Curve fitting and convergence for N_σ in axisymmetry.

and lower bound solution. Ref. [14] states that the upper and lower bounds stray at most 2.5% from the average. For the lower bound this means a minimum factor of $N_\sigma^{\text{lower}} = 0.6728$. This indicates that the finite element solution is well within the bounds.

11.2.2. Circular footing

In the case of a circular footing resting on a Hoek–Brown material the authors are not aware of any references that contain a solution with which the finite element solution can be compared.

The displacement–load relationship for the circular footing is very similar to that of the plane strain footing showed in Fig. 18.

The computed bearing capacity factors for the circular footing can be seen together with the fitted polynomials in Fig. 21. Again the factors drop as the mesh is refined. The lowest computed factors are $N_\sigma = 1.106$ and 1.096 for the associated and the non-associated material, respectively. Convergence values indicated of the polynomial curves are $N_\sigma^\infty = 1.101$ for the associated case and $N_\sigma^\infty = 1.094$ in the non-associated, respectively. The accuracy of the convergence value in the plane strain example, and similar convergence studies with a Mohr–Coulomb material, see Ref. [30], lead to the conclusion that the bearing capacity factor for a circular footing resting on an associated Hoek–Brown material with the parameters given in Table 4 is $N_\sigma = 1.10$.

The bearing capacity of the non-associated material is less certain, because of the non-uniqueness of the solutions for such materials, see e.g. Ref. [34].

12. Conclusions

A method for the plastic stress integration for a linear elastic–perfectly plastic Hoek–Brown material is presented. As opposed to earlier finite element implementations of this criterion the exact criterion is used, i.e. no rounding of the

corners or the apex is performed. The method is based on the return mapping scheme, i.e. a predictor–corrector scheme. The cornerstone for the formulation is to carry out all the manipulations in principal stress space and to use simple matrix algebra. In the principal stress space all the calculations needed to update the stress and to form the constitutive matrices simplify remarkably.

The iteration process needed to calculate the updated stress point reduces to solving a single scalar equation, which is easily done by the Newton–Raphson method.

The conditions for surface, line and apex returns can be given a geometrical meaning in principal stress space, and they are therefore easily implemented.

In connection with the calculation of the constitutive matrices the first and second derivatives of the yield function and the plastic potential are needed. The calculation of these simplify greatly in the principal stress space, as the Hoek–Brown criterion is formulated in principal stresses. Especially the formulae for the double singular constitutive matrix on a curve is simple compared to its formulation in general stress space, see [18].

The presented method is found to be far superior to a text book method of dealing with corner singularities. This is especially true for axisymmetric geometries, due to the great number of corner stress returns.

The method is validated by comparing some finite element results with results from the literature. The results are shown to converge toward previously reported solutions with great accuracy. For the axisymmetric footing, no value for the bearing capacity was found in the literature but the presented value is believed to be accurate.

Appendix A. Derivative of h_f used in a surface return

The function h_f is defined in Eq. (35). Its derivative, h'_f, is given by

$$h'_f = \frac{dh_f}{d\sigma_1} = \frac{d\alpha_r}{d\sigma_1} - \frac{d\alpha_s}{d\sigma_1}. \tag{A.1}$$

The slope of the connecting line, α_r, see Fig. 7, and its derivative are given by

$$\alpha_r = \frac{\sigma_3^C - \sigma_3^B}{\sigma_1^C - \sigma_1^B}, \quad \frac{d\alpha_r}{d\sigma_1} = \frac{k(\sigma_1^C - \sigma_1^B) - (\sigma_3^C - \sigma_3^B)}{(\sigma_1^C - \sigma_1^B)^2}, \tag{A.2}$$

where σ_3^C is taken from Eq. (33) and $k = \partial f/d\sigma_1$ is taken from Eq. (31).

The slope of the current plastic corrector direction, $\bar{\mathbf{s}}$, Eq. (34), and its derivative are given by

$$\alpha_s = \frac{s_3}{s_1} = \frac{vk_g - 1 + v}{(1-v)k_g - v}, \tag{A.3}$$

$$\frac{d\alpha_s}{d\sigma_1} = \frac{v(dk_g/d\sigma_1)((1-v)k_g - v) - (vk_g - 1 + v)(1-v)dk_g/d\sigma_1}{((1-v)k_g - v)^2}, \tag{A.4}$$

where $k_g = \partial g/d\sigma_1$ is taken from Eq. (32). The derivative of k_g is given by

$$\frac{dk_g}{d\sigma_1} = (1-a_g)\frac{a_g m_g^2}{\sigma_{ci}}\left(s_g - m_g\frac{\sigma_1}{\sigma_{ci}}\right)^{a_g - 2}. \tag{A.5}$$

Appendix B. Return to curve ℓ_1 i.e. to triaxial compressive corner

The intersection of the Hoek–Brown surface and the triaxial compressive plane described by $\sigma_1 = \sigma_2$ forms a curve in principal stress space. The parametric equation of the curve is given in Eq. (11), which is repeated here for convenience

$$\ell_1: \quad \bar{\boldsymbol{\sigma}} = \begin{Bmatrix} \sigma_1 \\ \sigma_2 \\ \sigma_3 \end{Bmatrix} = \begin{Bmatrix} \sigma_1 \\ \sigma_1 \\ \sigma_1 - \sigma_{ci}\left(s - m_b\frac{\sigma_1}{\sigma_{ci}}\right)^a \end{Bmatrix} \tag{11}$$

with σ_1 being the parameter. The curve is illustrated in Fig. 4 and a stress return to ℓ_1 is illustrated in Fig. 6. The direction vector of the curve is given by differentiation as

$$\bar{\mathbf{r}}_1 = [1 \;\; 1 \;\; k]^T, \tag{B.1}$$

where k is defined in Eq. (31). The direction vector is shown in Fig. B.1. In the case of returning the stress to ℓ_1 the plastic potential also forms a curve, ℓ_1^g, see Fig. B.1, defined by the intersection of the plastic potential, Eq. (13), with the triaxial compressive plane, $\sigma_1 = \sigma_2$. The direction vector of this curve is analogously to (B.1) given by

$$\bar{\mathbf{r}}_1^g = [1 \;\; 1 \;\; k_g]^T, \tag{B.2}$$

where k_g is defined in (32). The potential line direction vector is shown in Fig. B.1.

When the stress is returned to the yield surface the flow rule, Eq. (26), shows that the plastic strain direction is perpendicular to the plastic potential. This is also a valid point when the stress return is to the curve, and this is the basis for the equation to be solved. This means that a

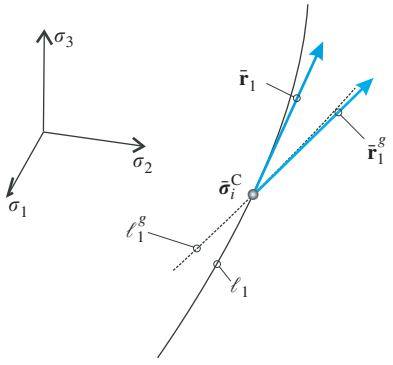

Fig. B.1. The curve ℓ_1 and its direction vector in the point $\bar{\boldsymbol{\sigma}}_i^C$. A part of the potential curve, ℓ_1^g and the corresponding direction vector, $\bar{\mathbf{r}}_1^g$ in the same point is also shown.

returned stress, σ_1^C, is sought which fulfils

$$h_1(\sigma_1^C) = (\bar{\mathbf{r}}_1^g)^T \Delta\bar{\boldsymbol{\varepsilon}}^p = 0, \tag{B.3}$$

where the plastic strain increment is found from Eq. (28) as

$$\Delta\bar{\boldsymbol{\varepsilon}}^p = \bar{\mathbf{D}}^{-1}\Delta\bar{\boldsymbol{\sigma}}^p. \tag{B.4}$$

Analogously to (36) the Newton–Raphson procedure for determining $\sigma_{1,i+1}^C$ is

$$\sigma_{1,i+1}^C = \sigma_{1,i}^C - \frac{h_1(\sigma_{1,i}^C)}{h_1'(\sigma_{1,i}^C)}. \tag{B.5}$$

The current value of the plastic corrector stress is given by

$$\Delta\bar{\boldsymbol{\sigma}}_i^p = \bar{\boldsymbol{\sigma}}^B - \bar{\boldsymbol{\sigma}}_i^C, \tag{B.6}$$

where $\bar{\boldsymbol{\sigma}}_i^C$ belongs to ℓ_1, i.e. it fulfils Eq. (11).

The derivative of h_1 is given by

$$h_1' = \frac{dh_1}{d\sigma_1} = \frac{d(\bar{\mathbf{r}}_1^g)^T}{d\sigma_1}\Delta\bar{\boldsymbol{\varepsilon}}^p + (\bar{\mathbf{r}}_1^g)^T\frac{d\Delta\bar{\boldsymbol{\varepsilon}}^p}{d\sigma_1}, \tag{B.7}$$

where

$$\frac{d(\bar{\mathbf{r}}_1^g)}{d\sigma_1} = \begin{bmatrix} 0 & 0 & \dfrac{dk_g}{d\sigma_1} \end{bmatrix}^T \tag{B.8}$$

with $dk_g/d\sigma_1$ given by Eq. (A.5).

The derivative of the plastic strain increment is given by

$$\frac{d\Delta\bar{\boldsymbol{\varepsilon}}^p}{d\sigma_1} = \bar{\mathbf{D}}^{-1}\frac{d\Delta\bar{\boldsymbol{\sigma}}^p}{d\sigma_1} = \frac{\bar{\mathbf{D}}^{-1}\begin{Bmatrix}\sigma_1^B - \sigma_1^C \\ \sigma_2^B - \sigma_2^C \\ \sigma_3^B - \sigma_3^C\end{Bmatrix}}{d\sigma_1} = -\bar{\mathbf{D}}^{-1}\bar{\mathbf{r}}_1. \tag{B.9}$$

In the above derivation use has been made of the fact that the updated stress, $\bar{\boldsymbol{\sigma}}^C$ belongs to ℓ_1, see Eq. (11), and that the corresponding derivative is given by Eq. (B.1).

As in the stress return to the surface, h_1, is not defined for $\sigma_1 > \sigma_t$. This means that the procedure outlined in Eq. (38) should be applied.

Appendix C. Return to curve ℓ_2 i.e. to the triaxial tensile corner

The intersection of the Hoek–Brown surface and the triaxial tensile plane described by $\sigma_2 = \sigma_3$ forms a curve in principal stress space. The parametric equation of the curve is given in Eq. (12), which is repeated here for convenience

$$\ell_2 : \bar{\boldsymbol{\sigma}} = \begin{Bmatrix}\sigma_1 \\ \sigma_2 \\ \sigma_3\end{Bmatrix} = \begin{Bmatrix} \sigma_1 \\ \sigma_1 - \sigma_{ci}\left(s - m_b\dfrac{\sigma_1}{\sigma_{ci}}\right)^a \\ \sigma_1 - \sigma_{ci}\left(s - m_b\dfrac{\sigma_1}{\sigma_{ci}}\right)^a \end{Bmatrix} \tag{12}$$

with σ_1 being the parameter. The curve is illustrated in Fig. 4 and a stress return to ℓ_2 is illustrated in Fig. 6. The direction vector of the curve is given by differentiation as

$$\bar{\mathbf{r}}_2 = [1 \;\; k \;\; k]^T, \tag{C.1}$$

where k is defined in Eq. (31).

The corresponding plastic potential direction vector and its derivative are given by

$$\bar{\mathbf{r}}_2^g = \begin{Bmatrix}1 \\ k_g \\ k_g\end{Bmatrix} \quad \text{and} \quad \frac{d\bar{\mathbf{r}}_2^g}{d\sigma_1} = \begin{Bmatrix} 0 \\ \dfrac{dk_g}{d\sigma_1} \\ \dfrac{dk_g}{d\sigma_1}\end{Bmatrix}. \tag{C.2}$$

The procedure of returning the stress to ℓ_2 is completely analogous to the stress return to ℓ_1, with $\bar{\mathbf{r}}_2$ replacing $\bar{\mathbf{r}}_1$ and $\bar{\mathbf{r}}_2^g$ replacing $\bar{\mathbf{r}}_1^g$.

Appendix D. Convergence rate

A rigourous proof that the presented constitutive matrix is in indeed the consistent constitutive matrix will not be given here. Instead and indication of the efficiency will be given.

In the computational example presented in Section 11 the average number of global equal equilibrium iterations was between 5 and 6 for most calculations. For comparison purposes some of the calculations were also carried out using the infinitesimal constitutive matrix. This matrix is found by replacing $\mathbf{D}^c$ with the elastic stiffness, $\mathbf{D}$ in Eqs. (59) and (70). The average number of global equilibrium iterations then soars to more than 100, which indicates the efficiency of the proposed constitutive matrix.

References

[1] Hoek E, Brown ET. Empirical strength criterion for rock masses. J Geotech Eng 1980;106:1013–35.
[2] Hoek E, Carranza-Torres C, Corkum B, Hoek–Brown failure criterion—2002 edition. In: Proceedings of the North American rock mechanics society meeting in Toronto in July 2002, 2002.
[3] Hoek E, Brown ET. Practical estimates of rock mass strength. Int J Rock Mech Min Sci 1997;34(8):1165–86.
[4] Rocscience Inc., RocLab version 1.021, ⟨www.rocscience.com⟩, 2006.
[5] Hoek E, Diederichs MS. Empirical estimation of rock mass modulus. Int J Rock Mech Min Sci 2006;43:203–15.
[6] Park K-H, Kim Y-J. Analytical solution for a circular opening in an elastic-brittle-plastic rock. Int J Rock Mech Min Sci 2006;43:616–22.
[7] Sharan SK. Exact and approximate solutions for displacements around circular openings in elastic-brittle-plastic Hoek–Brown rock. Int J Rock Mech Min Sci 2005;42:542–9.
[8] Serrano A, Olalla C, Jesús M. Stability of highly fractured infinite rock slopes with nonlinear failure criteria and nonassociated flow laws. Can Geotech J 2005;42:393–411.
[9] Carranza-Torres C, Fairhurst C. The elasto-plastic response of underground excavations in rock masses that satisfy the Hoek–Brown failure criterion. Int J Rock Mech Min Sci 1999;36:777–809.
[10] Serrano A, Olalla C, González J. Ultimate bearing capacity of rock masses based on the modified Hoek–Brown criterion. Int J Rock Mech Min Sci 2000;37:1013–8.
[11] Hoek E. Estimating Mohr–Coulomb friction and cohesion values from the Hoek–Brown failure criterion. Int J Rock Mech Min Sci Geomech Abstr 1980;34(8):227–9.

[12] Sofianos AI, Nomikos PP. Equivalent Mohr–Coulomb and generalized Hoek–Brown strength parameters for supported axisymmetric tunnels in plastic or brittle rock. Int J Rock Mech Min Sci 2006;43:683–704.
[13] Priest SD. Determination of shear strength and three-dimensional yield strength for the Hoek–Brown criterion. Rock Mech Rock Eng 2005;38(4):299–327.
[14] Merifield RS, Lyamin AV, Sloan SW. Limit analysis solutions for the bearing capacity of rock masses using the generalised Hoek–Brown criterion. Int J Rock Mech Min Sci 2006;43:920–37.
[15] Pan XD, Hudson JA. A simplified three dimensional Hoek–Brown yield criterion. In: Romana M, editor. Proceedings of the international society of rock mechanics (ISRM) symposium. Rotterdam: A.A. Balkema; 1988. p. 95–103.
[16] Wan RG. Implicit integration algorithm for Hoek–Brown elastic–plastic model. Comput Geotech 1992;14:1992.
[17] Owen DJR, Hinton E. Finite elements in plasticity: theory and practice. Swansea, UK: Pineridge Press Limited; 1980.
[18] Crisfield MA. Non-linear finite element analysis of solids and structures, vol. 2: advanced topics. New York: Wiley; 1997.
[19] Marinos P, Hoek E. GSI: a geologically friendly tool for rock mass strength estimation. In: Proceedings of the GeoEng2000 at the international conference on geotechnical and geological engineering, Melbourne. Lancaster: Technomic Publishers; 2000. p. 1422–46.
[20] Marinos V, Marinos P, Hoek E. The geological strength index: applications and limitations. Bull Eng Geol Environ 2005;64:55–65.
[21] Sloan SW, Abbo AJ, Sheng D. Refined explicit integration of elastoplastic models with automatic error control. Eng Comput 2001;18(1/2):121–54.
[22] Nagtegaal JC. On the implementation of inelastic constitutive equations with special reference to large deformation problems. Int J Numer Meth Eng 1982;33:469–84.
[23] Simo JC, Taylor RL. Consistent tangent operators for rate-independent elastoplasticity. Comput Meth Appl Mech Eng 1985;48:101–18.
[24] Krieg RD, Krieg DB. Accuracies of numerical solution methods for the elastic-perfectly plastic model. ASME J Pressure Vessel Technol 1977;(99):510–5.
[25] Larsson R, Runesson K. Implicit integration and consistent linearization for yield criteria of the Mohr–Coulomb type. Mech Cohesive Frictional Mater 1996;1:367–83.
[26] Rosati L, Valoroso N. A return map algorithm for general isotropic elasto/visco-plastic materials in principal space. Int J Num Meth Eng 2004;60:461–98.
[27] Clausen J, Damkilde L, Andersen L. Efficient return algorithms for associated plasticity with multiple yield planes. Int J Numer Meth Eng 2006;66(6):1036–59.
[28] Koiter WT. Stress–strain relations uniqueness and variational theorems for elastic–plastic materials with a singular yield surface. Q Appl Math 1953;11:350–4.
[29] Clausen J, Damkilde L, Andersen L. An efficient return algorithm for non-associated plasticity with linear yield criteria in principal stress space. Comput Struct 2007;85:1795–807.
[30] Clausen J. Efficient non-linear finite element implementation of elasto-plasticity for geotechnical problems. Ph.D. thesis, Esbjerg Institute of Technology, Aalborg University, ⟨http://vbn.aau.dk/fbspretrieve/10557579/JClausenAfhandling⟩, 2007.
[31] Cook RD, Malkus DS, Plesha ME. Concepts and applications of finite element analysis. New York: Wiley; 1989.
[32] Clausen J, Damkilde L. Slope safety factor calculations with non-linear yield criterion using finite elements. In: Schweiger HF, editor. Numerical methods in geotechnical engineering. London: Taylor & Francis Group; 2006. p. 491–6.
[33] Rocscience Inc., Plasticity Models in Phase2, ⟨www.rocscience.com/downloads/phase2/webhelp⟩, 2006.
[34] Vermeer PA. The orientation of shear bands in biaxial tests. Géotechnique 1990;40(2):223–36.